Time-resolved ion flux measurements in pulsed, electron-beam-generated plasmas

S. G. Walton,* D. Leonhardt, D. D. Blackwell, R. F. Fernsler, D. P. Murphy, and R. A. Meger
Plasma Physics Division, Naval Research Laboratory, Washington, DC 20375
(Received 24 October 2001; published 2 April 2002)

Time-resolved ion flux and energy distributions were measured at an electrode located adjacent to pulsed, electron-beam-generated plasmas in argon and oxygen. Temporal variations in the incident Ar^+, O^+, and O_2^+ energy and flux were correlated to changes in the electron temperature and plasma density. The decay time of the oxygen plasma is found to be shorter than that of the argon plasma, which is understood by considering the different loss mechanisms of each ion species.

DOI: 10.1103/PhysRevE.65.046412 PACS number(s): 52.50.Dg, 52.55.Dy, 52.20.−j

Pulsed plasmas have been investigated for some time and are thought to be well suited for certain materials processing applications [1,2]. For this reason, experiments involving pulsed plasmas are numerous and not limited to a specific type of source [3–7]. One attractive feature of pulsed systems is the added control over the ion flux at the surface, which is introduced by taking advantage of the modulations in electron temperature, plasma density, and species profiles. In this work, we report the results of investigations using pulsed, electron-beam-generated plasmas in argon and oxygen. The experiments were performed in the Naval Research Laboratory's large area plasma processing system [8] which utilizes a well-collimated, high-energy electron beam to ionize the background gas and thus produce a plasma. Electron-beam-generated plasmas have several unique features [9,10], including high densities and cold electron distributions over the volume of the beam. In previous experiments [11] we have measured plasma densities above 10^{11} cm^{-3} and electron temperatures less than 1.5 eV. Outside the beam, the outwardly diffusing plasma interacts with the background gas and remotely located electrodes (or substrates). We present time-resolved ion energy distributions and flux measurements at a grounded electrode surface located adjacent to the beam. The results are correlated to the fundamental plasma parameters and demonstrate the role of simple gas-phase kinetics in the plasma decay.

The experimental apparatus, schematically represented in Fig. 1, has been described elsewhere [12], and will only be briefly discussed here. The electron beam is produced by a long hollow-cathode discharge [13]. The emergent beam, collimated by a 150 G magnetic field, passed through a slot in a grounded anode and then terminated at a grounded beam dump. The electron beam volume between the slotted anode and dump defines the plasma source region. For all measurements reported here, the beam pulse was 1.0 ms long with a repetition rate of 33 Hz, and the beam energy was nominally 1.0 kV. Pulsed plasmas were produced in either 90 mTorr of argon or 60 mTorr of oxygen.

Ion flux and energy distributions were measured at a stainless steel electrode located 1.0 cm from the beam edge using Hiden's EQP 300 Plasma Probe (Fig. 1). The probe is differentially pumped and consists of an electrostatic ion-energy analyzer (ESA) in series with a quadrupole mass spectrometer (QMS). Ions enter the probe through a 100 μm diameter aperture located in the center of the electrode. Ions passing through the aperture are first energy selected and then mass filtered prior to detection by a channeltron secondary-electron multiplier (SEM). The ESA selects ions of a given energy $E \pm \Delta E/2$, where ΔE is the resolution of the ESA.

Measurements were carried out using both a fixed and scanning gate on the probe output (SEM) such that only those ions arriving during the gate period were counted. To achieve a reasonable signal-to-noise ratio, the signal was accumulated over several hundred pulses. The probe was not calibrated to determine the flux at the electrode surface from the reported signal intensity. However, it is reasonable to compare relative signal intensities when the probe settings are held constant for a given set of experimental parameters.

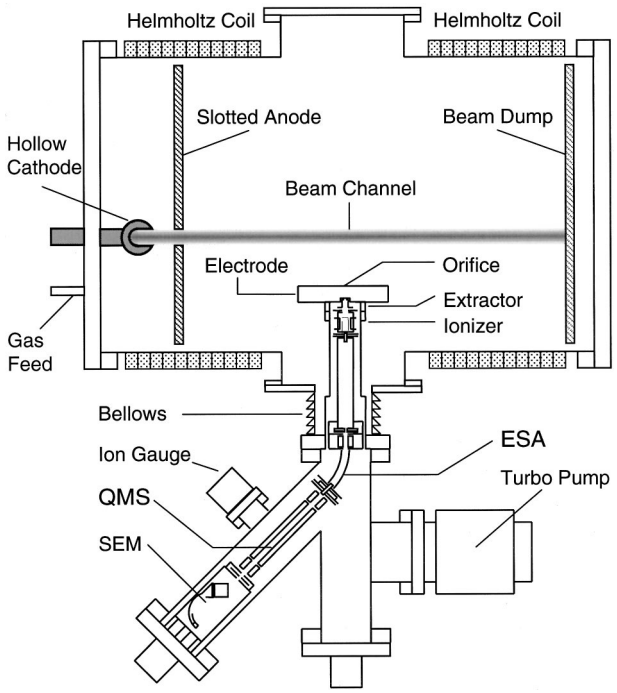

FIG. 1. Schematic diagram of the reactor and the plasma probe. The probe consists of an energy analyzer in series with a mass spectrometer.

*Permanent address: SFA, Inc., Largo, Maryland 20774. Electronic address: sgwalton@ccs.nrl.navy.mil

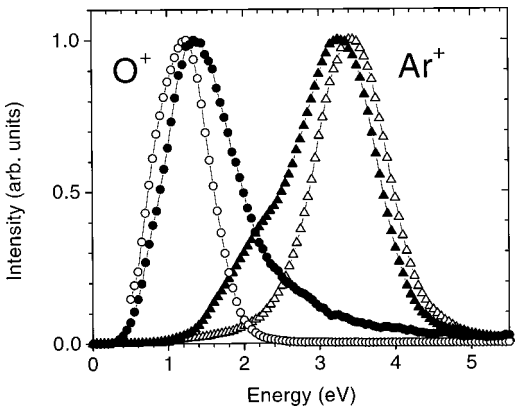

FIG. 2. Kinetic-energy distributions of Ar^+ (triangles) and O^+ (circles) sampled 1.0 cm from pulsed, electron-beam-generated plasmas in 90 mTorr of argon and 60 mTorr of oxygen, respectively. The distributions are accumulated during the steady-state period of the plasma (open symbols) and over all times for which there is a significant flux (solid symbols).

Shown in Fig. 2 are the Ar^+ and O^+ energy distributions accumulated over two fixed gate time periods. The first period extended from 200 μs to 1.0 ms, i.e., only while the electron beam was on and the plasma was in steady state. For the second period, the time window was expanded to include all times for which there was a significant flux, that is to say, the entire ''active glow'' and ''afterglow'' periods.

The time- and energy-resolved flux of each ion species is shown in Figs. 3 and 4. For these measurements, the ESA was set to pass a fixed energy ($\pm\Delta E/2$) and the SEM signal was monitored by a scanning, gated pulse counter. The flux was accumulated during a 10 μs gate that was scanned in steps of 10 μs. Note that the zero of the abscissa is defined by the front of the hollow-cathode pulse and the data are offset, in part, by the ion transit time in the probe ($\approx$45 μs for O^+ and $\approx$70 μs for Ar^+). Shown in Fig. 5 is the total time-resolved flux of each ion, which is approximated by summing the time- and energy-resolved signals of Figs. 3 and 4. Here we have assumed that, given the energy steps

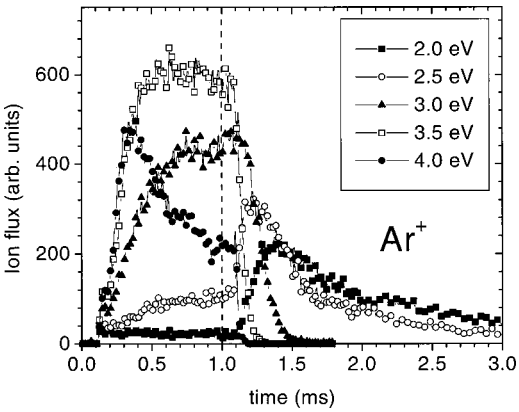

FIG. 3. Time-resolved Ar^+ flux measurements at various incident ion energies ($\pm$0.25 eV) for pulsed plasmas in 90 mTorr of argon. The dashed line indicates the end of the electron beam pulse (t=1.0 ms).

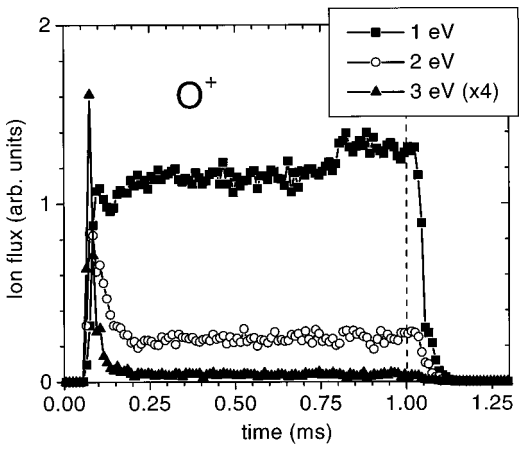

FIG. 4. Time-resolved O^+ flux measurements at various incident ion energies ($\pm$0.5 eV) for pulsed plasmas in 60 mTorr of oxygen.

and resolution (see figure captions), the sum is an accurate representation of the total time-resolved flux.

The shape and average energy of the distributions in Fig. 2 depend upon the time over which the distributions are accumulated, indicating that the incident ion flux and energy are time dependent. The details of these time dependencies are evident in the time-resolved flux measurements of Figs. 3 and 4, and the features of each energy distribution are readily correlated with these flux measurements. In argon, for example, when longer accumulation periods are used, the low-energy component (<3.0 eV) of the Ar^+ distribution (Fig. 2) is attributed to the flux of ions that peaks in intensity for times longer than 1.0 ms. In oxygen, the bias toward higher energies in the O^+ distribution (Fig. 2) results from the inclusion of ions arriving in times less than 200 μs. In both plasmas, the energy is found to reach a maximum early in time and then decay to a constant value during the pulse. After the beam is extinguished, the energies decrease and the ion signal decays.

Consider now the relationship of the measured quantities to the fundamental plasma properties, namely, the electron temperature (T_e) and the plasma density (n_0). For a colli-

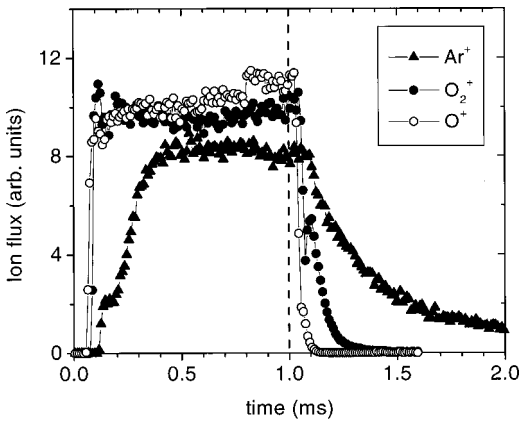

FIG. 5. The time-resolved, total ion flux of Ar^+, O^+, and $O_2{}^+$. The total flux is estimated by summing the time- and energy-resolved fluxes from Figs. 3 and 4.

sionless sheath, the incident ion energy E_i is determined by the ion kinetic energy at the presheath-sheath boundaryE_{ps} and the potential drop across the sheath V_s, and is given by [14]

$$E_i = E_{ps} + eV_s = kT_e[1/2 + \ln\sqrt{M_i/2\pi m_e}], \tag{1}$$

where k is Boltzmann's constant, M_i is the ion mass, and m_e is the electron mass. In separate experiments [11], the steady-state T_e is found to be $\approx$1.0 eV in argon and $\approx$0.3 eV in oxygen. The maximum ion energies in the energy distributions taken during the steady state (Fig. 2) agree with these values according to Eq. (1). Possible causes for the spread in energies below the maximum value are spatial and temporal variations in T_e and collisions within the sheath.

The ion flux Γ_i leaving the plasma can be expressed as [15]

$$\Gamma_i = \Gamma_e = n_s u_b = A n_0 \sqrt{kT_e/M_i}, \tag{2}$$

where $u_b = (kT_e/M_i)^{1/2}$ is the Bohm velocity and n_s is the number density at the presheath-sheath boundary which is assumed to be proportional to the bulk plasma density ($n_s = An_0$) [16].

By correlating the ion energies and signal intensities with the electron temperature and plasma density from Eqs. (1) and (2), we can infer a time-dependent description of the plasma. From the ion energies, the electron temperature spikes early in time and then settles to a steady-state value. During this time, the ion flux and the plasma density build to steady-state values. Once the beam is turned off, the electron temperature and the plasma density decay. Similar behavior has been observed in other pulsed plasmas in oxygen [17] and argon [7,18] and is compatible with global models [15] and simulations [19] employed to describe such plasmas.

While the variations in the ion flux for oxygen and argon plasmas are qualitatively similar, the time scales differ. This is well illustrated in the total ion flux measurements (Fig. 5) and in particular by the characteristic decay times of the signal. The decay time for the Ar^+ signal is greater than the decay times for both the O^+ and $O_2{}^+$, which differ as well. These differences may be understood in terms of the diffusion, electron-ion recombination, and charge exchange rates. Note that in these oxygen plasmas, the formation of negative ions is negligible [20] and so, unlike other electronegative plasmas [15,21], negative ions have no impact on the plasma decay.

To understand the plasma decay, consider the evolution of the density $n_i(t)$ for a given ion species (i):

$$\frac{dn_i}{dt} = S_i - k_r n_e n_i - k_c n_g n_i - \frac{D_{ai}}{l^2} n_i, \tag{3}$$

where S_i is the gas ionization rate, k_r is the electron-ion recombination coefficient, k_c is the ion destruction coefficient due to charge exchange, D_{ai} is the ambipolar diffusion constant, l is the source-electrode distance, n_g is the neutral density, and n_e is the electron density. If the beam is turned off at $t=0$, Eq. (3) reduces to,

$$\frac{dn_i}{dt} = -k_r n_e n_i - \beta n_i \tag{4}$$

where $\beta = [k_c n_g + (D_{ai}/l^2)]$. For the dominant ion species, we can set $n_i = n_e$ and then directly integrate Eq. (4) to obtain

$$t(n_i) = \frac{1}{\beta}\ln\left(\frac{n_{SS}(k_r n_i + \beta)}{n_i(k_r n_{SS} + \beta)}\right), \tag{5}$$

where $n_{SS} = n_i(0)$ is the steady-state plasma density. The time for $n_i(t)$ to drop by one e-fold is therefore

$$\tau_e = \frac{1}{\beta}\ln\left[e\left(\frac{k_r}{e} + \frac{\beta}{n_{SS}}\right) \Big/ \left(k_r + \frac{\beta}{n_{SS}}\right)\right]. \tag{6}$$

In order to compute the decay time τ_e, we need to determine n_{SS}, k_r, and β. The steady-state plasma density has been measured under similar conditions [11] and was found to be $n_{SS} \sim 10^{11}$ cm^{-3}. The electron-ion recombination rate coefficient is small for atomic ions [22] compared to that for molecular ions [23]: $k_r \sim 10^{-13}$ cm^3 s^{-1} for Ar^+ and O^+ versus $k_r \sim 10^{-8}$ cm^3 s^{-1} for $O_2{}^+$. Magnetization of the plasma electrons reduces the ambipolar diffusion coefficient [24] to a value of $D_{ai} \sim 10^3$ cm^2 s^{-1} for all ions of interest and it is assumed to be nearly constant over the time range considered. Considering only destructive charge exchange reactions and ignoring all interactions with impurities, the reaction of interest here ($O^+ + O_2 \rightarrow O + O_2{}^+$) has a rate coefficient [23] of $k_c \sim 10^{-11}$ cm^3 s^{-1}.

For Ar^+ and O^+, $k_r \ll \beta/n_{SS}$ and therefore Eq. (6) reduces to

$$\tau_e \approx 1/\beta. \tag{7}$$

For Ar^+, diffusion is the dominant loss mechanism since there is no destruction via charge exchange, and thus $\beta \sim (D_{ai}/l^2) \sim 10^3$ s^{-1}. In contrast, charge exchange is the dominant loss mechanism for O^+ where $\beta \sim k_c n_g \sim 10^4$ s^{-1}. For $O_2{}^+$, charge exchange is not important but electron-ion recombination is, depending on the plasma density n_{SS}. Assuming $n_{SS} \sim 10^{11}$ cm$^{-3} \sim (D_{ai}/l^2 k_r)$, and thus for $O_2{}^+$ Eq. (6) reduces to

$$\tau_e \approx \frac{1}{\beta}\ln\left(\frac{1+e}{2}\right) \approx \frac{1}{2\beta}, \tag{8}$$

where $\beta \sim (D_{ai}/l^2)$. Using Eqs. (7) and (8) we find the following:

$$\tau_e(Ar^+) \sim l^2/D_{ai} \approx 1.0 \text{ ms}, \tag{9}$$

$$\tau_e(O^+) \sim (k_c n_g)^{-1} \approx 0.1 \text{ ms}, \tag{10}$$

and

$$\tau_e(O_2{}^+) \sim l^2/2D_{ai} \approx 0.5 \text{ ms}. \tag{11}$$

The decay times from Eqs. (9)–(11) are in qualitative agreement with the decay in ion intensity observed in Fig. 5, where $\tau_e(Ar^+) > \tau_e(O_2^+) > \tau_e(O^+)$. The differences between the calculated and measured values are presumably due to the estimates and approximations used. In argon, for example, using a diffusion coefficient of $D_{ai} \approx 3 \times 10^3$ cm^2 s^{-1} in Eq. (9) would give better agreement with the observed decay. We have also assumed a constant electron temperature, which impacts the diffusion coefficients in both plasmas and the electron-ion recombination rate in the oxygen plasma. Nonetheless, the results are useful in understanding how the various reactions influence the plasma decay.

In summary, time-resolved ion energy distributions and ion fluxes from pulsed, electron-beam-produced plasmas in argon and oxygen were measured and used to develop a temporal profile of each plasma. The observed plasma decay was found to agree with a simple description based on gas-phase kinetics. In argon, the decay is dominated by diffusion while in oxygen, electron-ion recombination and charge exchange reactions are significant. In the future, we expect a more rigorous approach will allow us to account for all time-dependent features and the interactions within pulsed, electron-beam-generated plasmas.

This work was supported by the Office of Naval Research. D.D.B. gratefully acknowledges the support of the National Research Council.

[1] See, for example, N. Itagaki, A. Fukuda, T. Yoshizawa, M. Shindo, Y. Ueda, and Y. Kawai, Surf. Coat. Technol. **131**, 54 (2000).
[2] See, for example, S. Samukawa and T. Mieno, Plasma Sources Sci. Technol. **5**, 132 (1996).
[3] Lawrence J. Overzet and Foong Ying Leong-Rousey, Plasma Sources Sci. Technol. **4**, 432 (1995).
[4] T. Mieno and S. Samukawa, Plasma Sources Sci. Technol. **6**, 398 (1995).
[5] C. Charles and R. W. Boswell, J. Appl. Phys. **78**, 766 (1995).
[6] M. Baeva, X. Luo, B. Pfelzer, T. Repsilber, and J. Uhlenbusch, Plasma Sources Sci. Technol. **9**, 128 (2000).
[7] O. Zabeida, A. Hallil, M. R. Wertheimer, and L. Martinu, J. Appl. Phys. **88**, 635 (2000).
[8] W. M. Manheimer, R. F. Fernsler, M. Lampe, and R. A. Meger, Plasma Sources Sci. Technol. **9**, 370 (2000).
[9] R. F. Fernsler, W. M. Manheimer, R. A. Meger, J. Mathew, D. P. Murphy, R. E. Pechacek, and J. A. Gregor, Phys. Plasmas **5**, 2137 (1998).
[10] M. J. Kushner, W. Z. Collison, and D. N. Ruzic, J. Vac. Sci. Technol. A **14**, 2094 (1996).
[11] D. Leonhardt, S. G. Walton, D. D. Blackwell, W. E. Amatucci, D. P. Murphy, R. F. Fernsler, and R. A. Meger, J. Vac. Sci. Technol. A **19**, 1367 (2001).
[12] S. G. Walton, D. Leonhardt, D. D. Blackwell, R. F. Fernsler, D. P. Murphy, and R. A. Meger, J. Vac. Sci. Technol. A **19**, 1325 (2001).
[13] R. F. Fernsler, W. M. Manheimer, R. A. Meger, J. Mathew, D. P. Murphy, R. E. Pechacek, and J. A. Gregor, Phys. Plasmas **5**, 2137 (1998).
[14] M. A. Lieberman and A. J. Lichtenberg, *Principles of Plasma Discharges and Materials Processing* (Wiley, New York, 1994).
[15] M. A. Liebermann and S. Ashida, Plasma Sources Sci. Technol. **5**, 145 (1996).
[16] For example, see Ref. [14], Sec. 5.3.
[17] R. W. Boswell and D. Vender, Plasma Sources Sci. Technol. **4**, 534 (1995).
[18] S. Ashida, M. R. Shim, and M. A. Lieberman, J. Vac. Sci. Technol. A **14**, 391 (1996).
[19] R. W. Boswell and D. Vender, IEEE Trans. Plasma Sci. **19**, 141 (1991).
[20] In oxygen, T_e is too low for negative ions to form via dissociative attachment ($e + O_2 \rightarrow O + O^-$) and three-body attachment ($e + 2O_2 \rightarrow O_2 + O_2^-$) does not occur because the gas density is too low.
[21] D. Leonhardt, S. G. Walton, D. D. Blackwell, D. P. Murphy, R. F. Fernsler, and R. A. Meger, in *28th IEEE International Conference on Plasma Science Conference Record, June 2001*, IEEE Cat. No. 01CH37255, pp. 158.
[22] For example, see D. R. Bates and A. Delgarno, *Atomic and Molecular Processes* (Academic, New York, 1962).
[23] I. A. Kossyi, A. Y. Kostinsky, A. A. Matveyev, and V. P. Silakov, Plasma Sources Sci. Technol. **1**, 207 (1992).
[24] For example, see Ref. [14], Sec. 5.4